Check for updates

Fenton photocatalytic sponges for rapid separation of emulsified-oil/dyes†

Hongliang Zhang[a] and Zhiguang Guo ⓘ *[a,b]

It is challenging to effectively and swiftly address oil and dye pollution. Herein, AM/MAA/HNTs/β-FeOOH sponges with high adsorption performance and strong photocatalytic resistance to oil/dye pollution is reported. β-FeOOH loading increases the specific surface area of the whole material in HNTs, which improves the adsorption of dyes. Composites of HNTs/β-FeOOH of appropriate ratio can realize the adsorption of dyes ($C \leq 20$ mg L^{-1}) in 3 min. In addition, due to the photocatalytic properties of β-FeOOH, HNTs/β-FeOOH can also realize the photocatalytic degradation of methylene blue ($C = 30$ mg L^{-1}) in 30 min. The underwater superoleophobic properties of the AM/MAA/HNTs/β-FeOOH sponge is attributed to improvements of roughness and hydrophilicity. The modified sponge with its special wettability and good adsorption photocatalytic performance enables it to rapidly separate emulsion/dyes ($C <$ 10 mg L^{-1}). This study provides an alternative and effective solution for the problem of oil/dye contamination in complicated wastewater.

1. Introduction

With the rapid development of industry, the human ecological environment has been polluted. Typical pollutants include oil (in water pollution) and refractory dyes.[1] Compared with single oil–water pollution, oil–water pollutants containing dyes, as complex oil–water pollutants, are difficult to separate. Many technologies have been applied to the treatment of complex oil–water pollutants in industry, such as centrifugal separation technology,[2,3] electric separation technology,[4] adsorption separation technology,[5,6] air flotation separation technology,[7] membrane separation technology,[8,9] and so on. However, most of these techniques have the disadvantages of high energy consumption and high cost. Superoleophilic/superhydrophobic materials, with their special wetting state, exhibit excellent performances in the separation of complex oil–water pollutants.[10] However, as separation membranes, these materials are easily clogged during the separation process, and it is difficult to clean the highly viscous oil remaining on their surfaces after separation.[11] In contrast, superhydrophilic/underwater superoleophobic materials have the advantages of high separation efficiency,

low contamination, *etc.*[12] Compared with two-dimensional membrane materials, three-dimensional sponge materials have high porosity, which makes them superior in separating high-viscosity oil or complex oil–water pollutants. Therefore, there is an urgent need to develop multifunctional superhydrophilic/underwater superoleophobic sponges to purify complex oily wastewater.

Advanced oxidation processes (AOPs) are highly efficient in water treatment and show great potential in degrading a wide range of persistent organic pollutants.[13–16] The non-homogeneous Fenton-like reaction is an effective and economical AOP that mainly utilizes hydroxyl radicals or superoxide radicals to degrade difficult-to-degrade organics.[17,18] The combination of a Fenton photocatalyst and super hydrophilic/underwater superhydrophobic materials can not only significantly improve its antifouling performance, but also improve the treatment effect of complex oily wastewater. β-FeOOH is a promising non-homogeneous photo-Fenton catalyst, which has the advantages of good photo-Fenton catalytic performance (band gap of about 2.12 eV), excellent adsorption performance, is easy to synthesize, is low cost and has good chemical stability.[19,20] On the other hand, the abundance of high-energy surface hydroxyl groups inherent in β-FeOOH contributes to the trapping of water molecules and the formation of a barrier layer, which can effectively prevent oil droplets from contacting the membrane surface during the separation process, thus enhancing the membrane's resistance to contamination.[21] The assembly of a polyphenol (tannic acid, TA)-poly(cationic) (polyethyleneimine, PEI)-metal ion (Fe^{3+}) layer by Yan's group on the surface of polyphenylene sulfide (PPS) substrates provided a double-crosslinked coating. The PPS/

[a] Ministry of Education Key Laboratory for the Green Preparation and Application of Functional Materials, School of Materials Science & Engineering and Hubei Key Laboratory of Polymer Materials, Hubei University, Wuhan 430062, People's Republic of China. E-mail: zguo@licp.cas.cn
[b] State Key Laboratory of Solid Lubrication, Lanzhou Institute of Chemical Physics, Chinese Academy of Sciences, Lanzhou 730000, People's Republic of China
†Electronic supplementary information (ESI) available. See DOI: https://doi.org/10.1039/d5lp00070j

TA-PEI/β-FeOOH composite membranes achieved excellent separation of various oils-in-water (O/W) emulsions. The PPS/TA-PEI/β-FeOOH membranes are super hydrophilic in air and super oleophobic underwater. These PPS/TA-PEI/β-FeOOH membranes have a strong photo-Fenton self-cleaning capacity for different O/W emulsions, with a flux recovery of the contaminated membranes that exceeds 90.3% when cleaned with visible light for 10 minutes.[22] However, realizing the rapid separation of complex oily wastewater still needs further discussion. Stable halloysite nanotubes have a strong adsorption capacity for soluble pollutants due to their extremely large specific surface area and electrical charge characteristics (positive/negative internal/external surface charge, respectively).[23] Due to the photocatalytic properties of β-FeOOH and the adsorption properties of halloysite nanotubes, these composites can be used for the removal of organic pollutants from aqueous bodies. The electrons and holes generated by β-FeOOH in the presence of light can trigger oxidation reactions, while the halloysite nanotubes provide a large specific surface area and numerous adsorption sites, which together promote the degradation and removal of pollutants.[24]

In this paper, AM/MAA/HNTs/β-FeOOH was synthesized by a hydrothermal method using a melamine sponge as a skeleton (Fig. 1). The resultant AM/MAA/HNTs/β-FeOOH sponge can realize the effective separation of various oil–water emulsions and highly soluble pollutants, in addition to the rapid purification of oil-containing wastewater with the simultaneous effective separation of various oil–water emulsions and highly soluble pollutants (e.g. MB). At the same time, the AM/MAA/HNTs/β-FeOOH sponge shows good stability and high chemical resistance to different corrosive media (acid/alkali).

2.   Materials and methods

2.1   Materials

Melamine sponge (0.012 g cm^{-3}) was purchased from a local store. Ferric chloride (FeCl$_3$, 99.0%) was obtained from Tianjin Jinnan Chemical Reagent Yard. Acrylamide (AM, ≥99.0%) was purchased from Aladdin. Methacrylic acid (MAA, 99.0%) was acquired from Anhui Zesheng Technology Co. Halloysite nanotubes (HNTs, 95%, diameter 0.1–0.4 μm, length <0.5 μm) were purchased from Xinlei Mineral Powder Processing Factory. Potassium persulfate (KPS, 99.5%), sodium hydroxide (NaOH, 98%) and hydrochloric acid (HCl, 38%) were purchased from Sinopharm Chemical Reagent Co.

2.2   Preparation of HNTs/β-FeOOH-x

The HNTs were first pretreated to remove impurities and water from them and to increase the number of active sites on their surfaces. A quantitative amount of FeCl$_3$ was added to 100 mL of deionized water, followed by ultrasonication for 5–10 min to ensure it was well dispersed. A beaker containing 100 mL of FeCl$_3$ solution was placed in a water bath at 80 °C for 4 h and then cooled to room temperature. Then, 10 mg mL^{-1} of HNTs was added to the above solution, and the pH value of the solution was adjusted to 10 with 0.1 mol L^{-1} NaOH solution, and the solution was fully reacted in a water bath at 80 °C for 2 h. The solution was aged at room temperature for 2 days. The powder was washed several times with deionized water and anhydrous ethanol until the supernatant was neutral, centrifuged, dried in an oven at 55 °C, and ground through a sieve. The obtained powder material was β-FeOOH-modified halloysite nanotubes (HNTs/β-FeOOH). The mass ratio of FeCl$_3$ to HNTs in the preparation process was defined as x. Modified powders with different mass ratios were denoted as HNTs/β-FeOOH-x.

2.3   Preparation of AM/MAA/HNTs/β-FeOOH-x

A polyurethane sponge was cleaned with deionized water and ethanol, respectively, and was dried at 30 °C for 3 h and then removed as a spare. Underwater superoleophobic sponges were prepared using the one-pot method. Deionized water (125 mL) was used to dissolve 6 wt% AM (relative to the total mass of the precursor solution), 0.3 M MAA (relative to the volume of
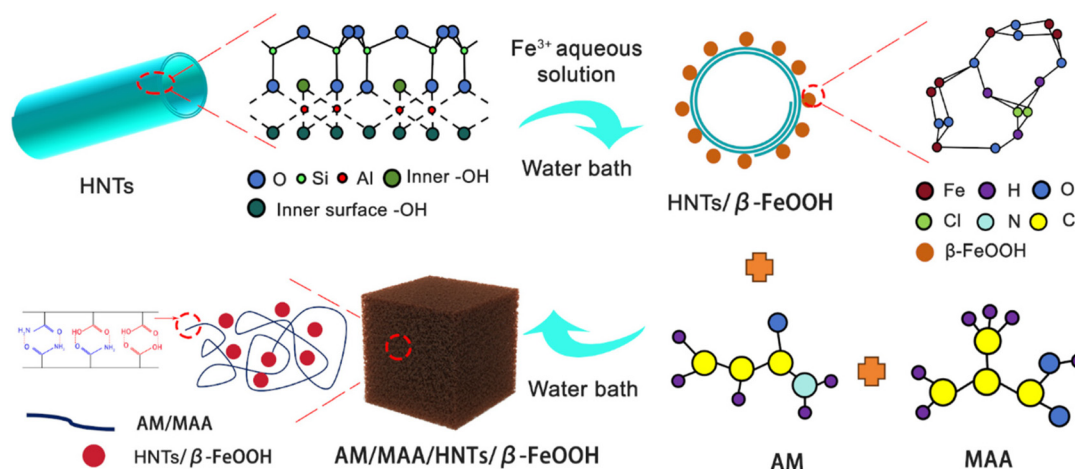

Fig. 1   Flow chart of AM/MAA/HNTs/β-FeOOH preparation.

the deionized water) and 2 wt% KPS (relative to the total mass of AM and MAA). Finally, 2 mg mL^{-1} HNTs/β-FeOOH-x was added to the AM/MAA/solution. The pretreated polyurethane sponge was then placed into the above precursor solution. The reaction was carried out at 60 °C for 2 h. The sponge was removed and washed with deionized water.

2.4 Characterization

Contact angles were characterized by a contact angle meter (Dataphysics, OCA25) with deionized water (10 μL) and dichloromethane (10 μL) used as probe liquids. The surface composition was analyzed using X-ray photoelectron spectroscopy (Physical Electronics, PHI-5702; USA) and binding energies were calibrated against contaminated carbon in air (C 1s: 284.8 eV). The crystallinity of the solid powders was determined by X-ray diffraction (XRD) on a Bruker D8 Advance diffractometer at a scanning rate of 5° min^{-1} under CuKα radiation (λ = 1.54 Å) at 40 kV and 40 mA. The potential values of HNTs and HNTs/β-FeOOH-x were tested at different pH values on a Zetasizer Nano ZS90 potential analyzer. The absorbance of the dyes after adsorption or photodegradation was measured on a UV-vis/NIR spectrophotometer (UV-vis/NIR, CLY21). The powder specific surface area and pore size were tested on a specific surface area and pore distribution meter (BET, MIC-2460).

2.5 Emulsion separation

A surfactant-stabilized oil–water emulsion was used to simulate oily wastewater and was prepared as follows: an oil phase (cyclohexane, dichloromethane, trichloromethane, soybean oil), 50 mg of sodium dodecyl sulfate, and water ($V_{water} : V_{oil}$ = 99 : 1) were combined and mechanically stirred for 6 h at 600 rpm. Immediately after preparation, it was subjected to separ-

ation. The emulsion particle size was characterized using a nanoparticle size potential analyzer (Nano ZS 90). A vacuum pump was used for the oil–water emulsion separation experiments with a filtration pressure of 0.1 bar:

$$J = \frac{V}{Atp} \tag{1}$$

where V (L) represents the filtrate volume, A (m^2) denotes the effective area, p (bar) signifies the transmembrane pressure, t (h) represents the operation time and J is the filtration flux (L·m^{-2}·h^{-1}·bar^{-1}). The filtrated water was collected, and its residual oil content was detected using a UV-vis spectrophotometer (TU1810). The separation efficiency (R) was calculated by using the following equation:

$$R = \frac{C_0 - C_f}{C_0} \times 100\% \tag{2}$$

where C_0 and C_f are the oil content in the O/W emulsion and filtrate, respectively.

3. Results and discussion

3.1 Compositional analysis

The XRD patterns of β-FeOOH, HNTs and the PDF card for β-FeOOH are shown in Fig. 2a. The diffraction peaks with 2θ values of 11.8°, 16.7°, 26.7°, 35.1°, 39.2°, 46.4°, and 55.9° correspond to the (110), (200), (310), (211), (301), (411), and (521) crystal planes of β-FeOOH, respectively, which corresponds to the PDF#34-1266.[25] The XRD spectrum of HNTs showed that pretreatment did not destroy the structure of the HNTs.[26] The elemental valence states of β-FeOOH, HNTs and HNTs/β-FeOOH were further analyzed by XPS to verify the
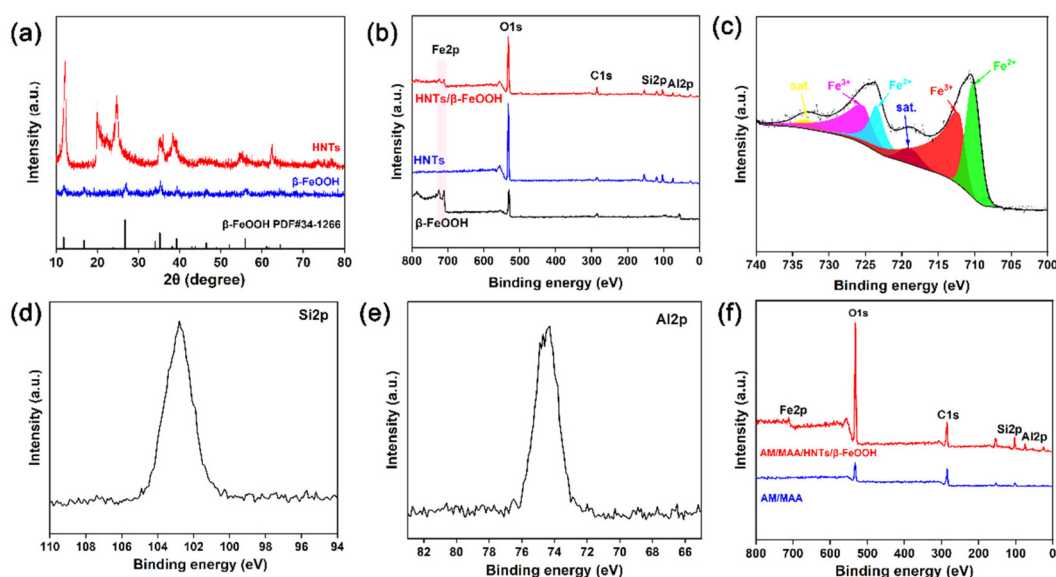

Fig. 2 (a) XRD diffraction patterns and (b) full XPS spectra of β-FeOOH, HNTs and HNTs/β-FeOOH. (c) XPS Fe 2p spectra of HNTs/β-FeOOH. XPS spectra of (d) Si 2p and (e) Al 2p of HNTs/β-FeOOH. (f) XPS full spectrum of AM/MAA/HNTs/β-FeOOH.

loading of β-FeOOH. As can be seen from Fig. 2b, the absorption peaks with binding energies located at 102.9 eV and 74.7 eV in the XPS spectrogram of HNTs/β-FeOOH are attributed to Si 2p and Al 2p, respectively (Fig. 2d and e). The Fe 2p XPS spectra of HNTs/β-FeOOH are shown in Fig. 2c. Two of the satellite peaks are characteristic peaks of mixed-valence Fe materials located at 718.4 eV and 732.9 eV, respectively. The fitted peaks located at 710.5 eV and 724.2 eV are attributed to Fe^{2+}. In addition, the fitted peaks located at 712.7 eV and 726.7 eV were attributed to Fe^{3+}.[27] These peaks confirm that β-FeOOH was successfully loaded onto HNTs. Compared with the spectral profile of the AM–MAA sponge, the AM/MAA/HNTs/β-FeOOH profile showed characteristic absorption peaks consistent with HNTs/β-FeOOH, which proved the successful preparation of the AM/MAA/HNTs/β-FeOOH sponge (Fig. 2f).

3.2 Wettability and stability

It is well known that the antifouling property of a material is related to the wettability of its surface.[28] The gel produced by the hydrothermal reaction of MAA and AM was used as a binder to adhere HNTs/β-FeOOH. HNTs/β-FeOOH increased the surface roughness of the material (Fig. S1†) while the abundant hydroxyl groups on its surface increased the surface energy.[29] This makes AM/MAA/HNTs/β-FeOOH exhibit underwater superoleophobicity with an underwater oil contact angle of 153° (Fig. 3a). Usually the stability of the material is the basis of the application. AM/MAA/HNTs/β-FeOOH was immersed in aqueous solutions with different pH values to test its stability in extreme environments. As shown in Fig. 3b, the AM/MAA/HNTs/β-FeOOH sponge did not change color and the acidic solution remained transparent and clear after it was immersed in acid (pH = 2) for 18 h. In contrast, when the AM/MAA/HNTs/β-FeOOH sponge was placed in an alkaline environment, the solution became turbid after 18 h of immersion, and fallen particles of HNTs/β-FeOOH powder were visible at the bottom of the beaker. This is mainly attributed to the fact that the copolymerization product of the reaction between MAA and AM is resistant to acids but not bases.[30]
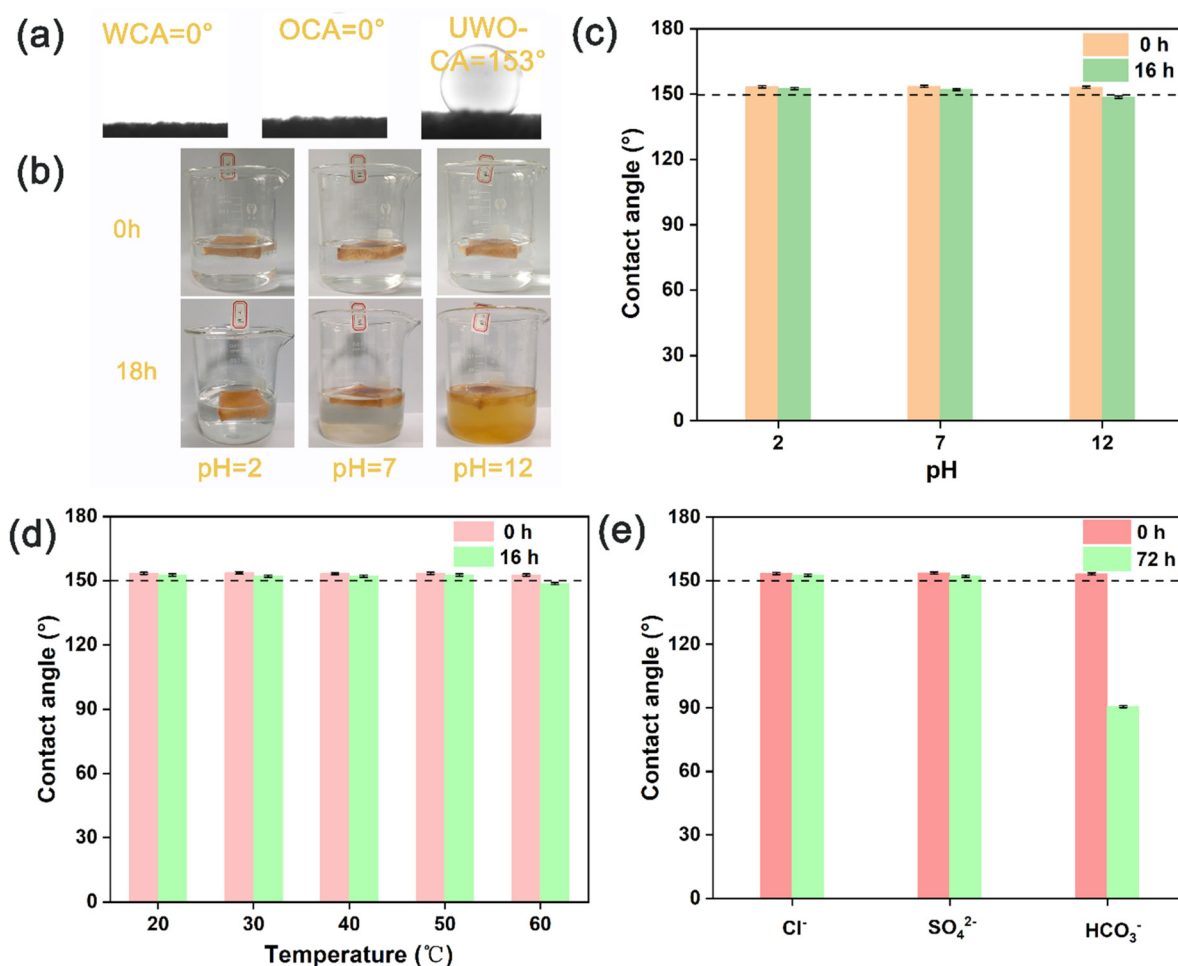

Fig. 3 (a) Oil contact angle of AM/MAA/HNTs/β-FeOOH sponge in air and underwater. (b) Photographs of the AM/MAA/HNTs/β-FeOOH sponge immersed in aqueous solutions of different pH. (c) Surface wettability of the sponge after immersion in solutions of different pH. Surface wettability of the AM/MAA/HNTs/β-FeOOH sponge after (d) immersion at different temperatures for 16 hours and (e) immersion in different ionic solutions (20 mM) for 72 hours.

© 2025 The Author(s). Published by the Royal Society of Chemistry

RSC Appl. Polym., 2025, **3**, 916–925 | **919**

This also led to a decrease in the underwater oil contact angle after the chemical stability test, except for the acid-soaked samples (Fig. 3c). In addition, temperature has a relatively small effect on AM/MAA/HNTs/β-FeOOH (Fig. 3d). In order to further cope with complex environments, its stability in different ionic solutions (Cl^-, SO_4^{2-}, HCO_3^-) was tested. After soaking in HCO_3^- solution for 72 hours, most of the HNTs/β-FeOOH particles were completely detached, and the AM/MAA/HNTs/β-FeOOH had turned white. After soaking in the other two ionic solutions for 72 hours, the AM/MAA/HNTs/β-FeOOH can still maintain its underwater oil-repellent state (Fig. 3e). Overall, AM/MAA/HNTs/β-FeOOH exhibits good stability.

3.3 Adsorption and photo-Fenton catalyzed degradation

For fast adsorption and photo-Fenton-catalyzed degradation, we prepared HNTs/β-FeOOH-x powders with different mass ratios of β-FeOOH to HNTs (x = 1, 0.8, 0.6, 0.4, 0.2). The adsorption effect of different powders for MB was first discussed. The powders were put into cationic solutions of methylene blue dye (MB: 20 mg L^{-1}, pH = 8.6, HNTs/β-FeOOH-

x: 2 mg mL^{-1}), and a stirring table was set to rotate the mixtures at a speed of 300 rpm. The adsorption of MB by the different powders and their effect on the dye are shown in Fig. 4a, revealing that the HNTs powder has a better adsorption effect on the methylene blue solution within 5 min, and its MB removal rate is up to 53.1% (Fig. 4b). Three reasons can be given to explain this phenomenon. (1) HNTs have a very large specific surface area (20.0516 m^2 g^{-1}); (2) under an alkaline environment, HNTs show negative electronegativity with a zeta value of −37.933 mV (Table S2†), and there is a charge attraction with the cationic MB. (3) The aromatic ring, and the nitrogen and oxygen atoms of MB molecules are attracted to the single bond OH group of the HNTs through hydrogen bonding.[31] The HNTs showed fast and then slow adsorption during the adsorption process, specifically, the adsorption was faster during the 0–1 min stage, and slowed down during the 1–5 min stage. The above phenomenon may be attributed to the large number of adsorption sites on the surfaces of the HNTs and the large concentration of methylene blue, which led to the fast adsorption rate in the 0–1 min stage. With the decrease of adsorption sites and MB concentration, the
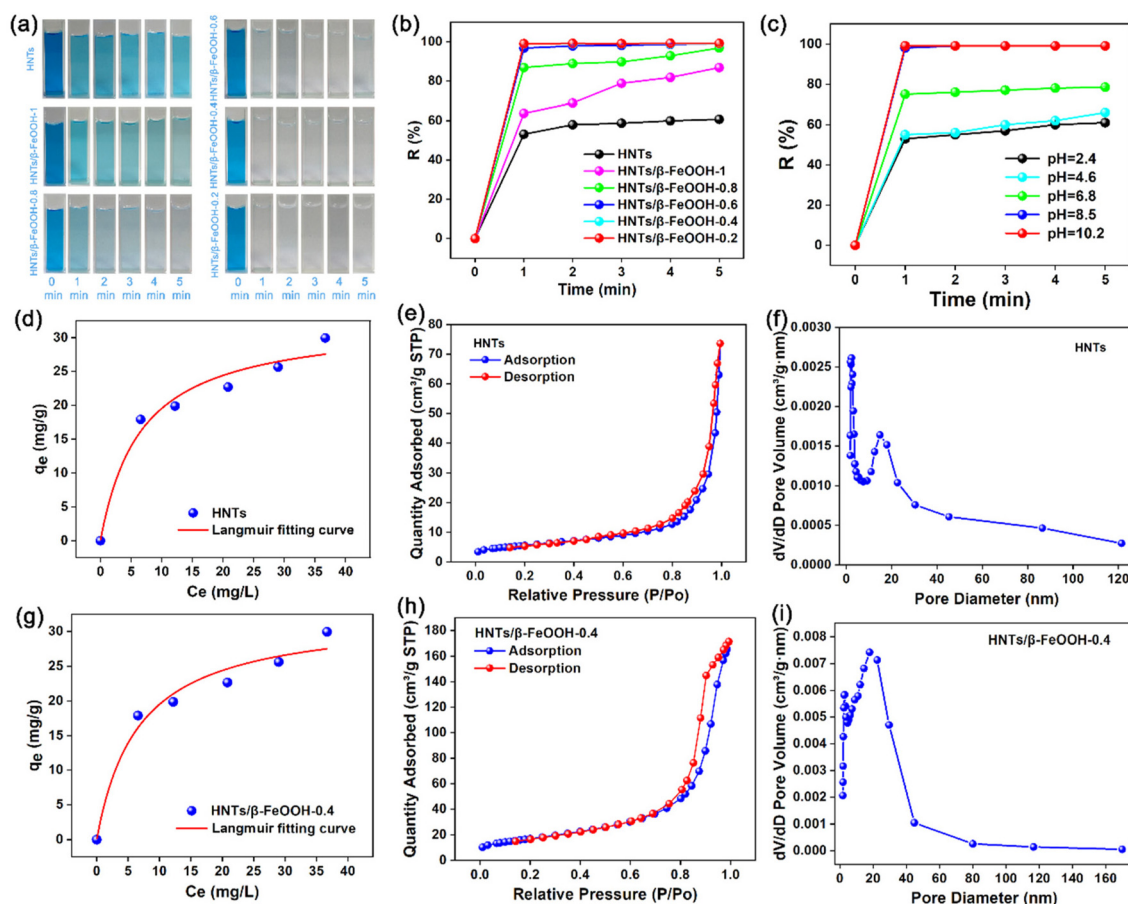

Fig. 4 (a) Photographs of the adsorption effect of powder HNTs/β-FeOOH-x on MB solution (20 mg L^{-1}) within 5 min. (b) Removal rate of MB by HNTs/β-FeOOH-x. (c) Removal rate of MB by HNTs/β-FeOOH-0.4 from solutions (20 mg L^{-1}) at different pH values. Langmuir adsorption fitting curves for HNTs (d) and HNTs/β-FeOOH-0.4 (g). Adsorption–desorption curves for HNTs (e) and HNTs/β-FeOOH-0.4 (h). Pore sizes of HNTs (f) and HNTs/β-FeOOH-0.4 (i).

adsorption rate decreased. In contrast, HNTs/β-FeOOH-x adsorbed better than HNTs in the 0–1 min stage. In particular, HNTs/β-FeOOH-0.4 and HNTs/β-FeOOH-0.2 can realize rapid MB adsorption performances with a removal rate as high as 99% in as little as 1–2 min (Fig. 4b). The nitrogen adsorption–desorption isotherms and pore size distributions of HNTs and HNTs/β-FeOOH-0.4 are shown in Fig. 4e, f, h, and i. As can be seen from Fig. 4e and h, the overall trend of adsorption–desorption of HNTs and HNTs/β-FeOOH-0.4 is similar, with the curve at the low-pressure end rising slowly; the curve in the medium-pressure section rises more; and the high-pressure section exhibits a clear hysteresis loop, which is in agreement with the performance of typical V-band H3-type hysteresis curves,[32] confirming that the HNTs/β-FeOOH-0.4 consists of a lax sheet-like structure of slit-like pores. As shown in Fig. 4d and g, HNTs and HNTs/β-FeOOH-0.4 have a large number of mesopores with pore diameters between 2 and 50 nm, and a small number of macropores with pore diameters >50 nm. Combined with the results in Table S1,† it can be seen that after the β-FeOOH modification of HNTs, the pore size of

HNTs/β-FeOOH-0.4 decreased but the specific surface area increased, and the total adsorption performance was further improved. In summary, the very large specific surface area was the main reason for the rapid adsorption of HNTs/β-FeOOH-0.4 in the short term. In addition, the total adsorption amount of modified HNTs/β-FeOOH-0.4 was not enhanced by fitting a Langmuir curve, and the maximum adsorption amount was 32.581 mg g^{-1}. The possible reason for this phenomenon is that the pore volume of modified powder HNTs/β-FeOOH-0.4 is extremely small.[24] With respect to the adsorption of MB in different pH environments, the adsorption of MB by HNTs/β-FeOOH-0.4 in an alkaline environment was significantly better than that in an acidic environment. This was due to the different zeta potentials.[33]

The AM/MAA/HNTs/β-FeOOH-0.4 sponge was selected to continue the subsequent tests considering the photo-Fenton reaction. As shown in Fig. 5a–d, the porous substrate sponges showed adsorption at 500 rpm, and the removal of MB was 49%, 32%, and 18% at concentrations of 10 mg L^{-1}, 20 mg L^{-1}, and 30 mg L^{-1}, respectively. The AM/MAA/HNTs/
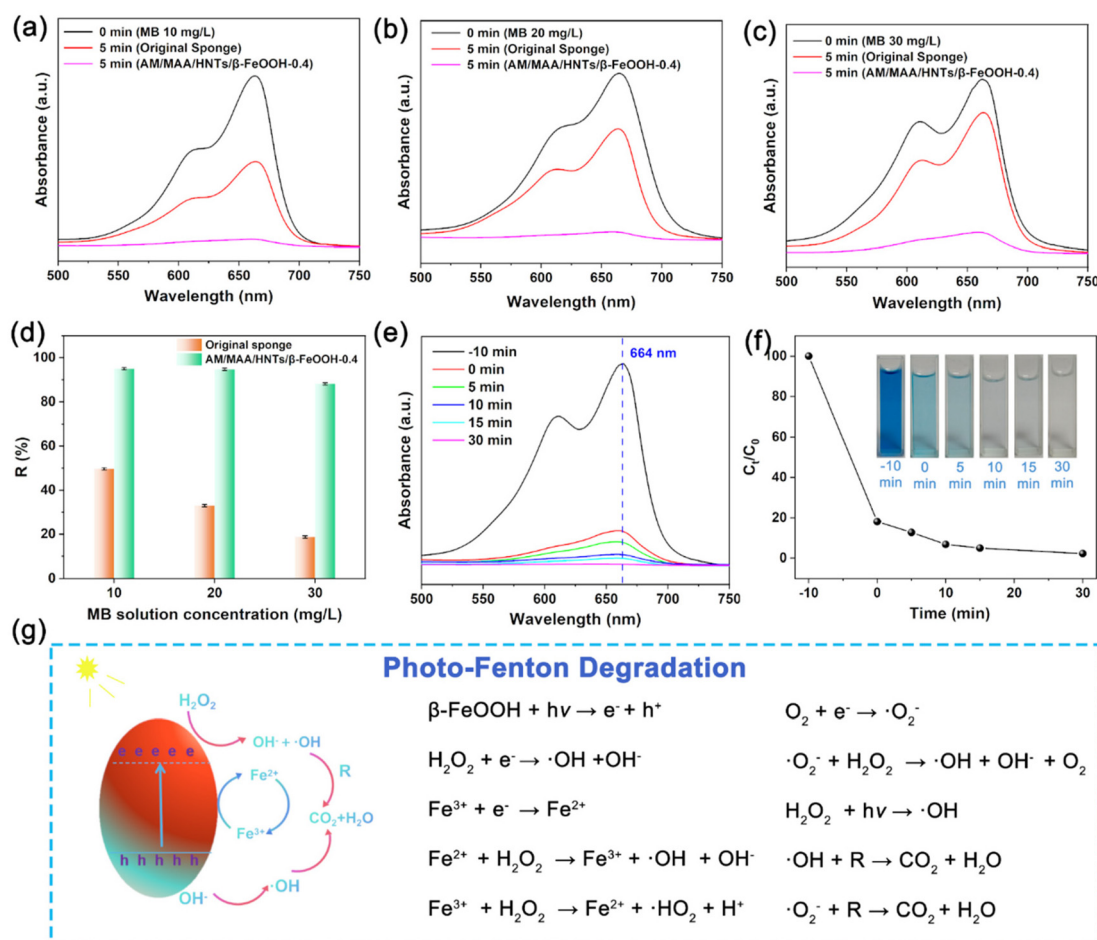

Fig. 5 UV-vis absorption spectra for different concentrations of MB in the presence of a pristine sponge and an AM/MAA/HNTs/β-FeOOH-0.4-modified sponge. (a) 10 mg L^{-1} MB, (b) 20 mg L^{-1} MB, (c) 30 mg L^{-1} MB. (d) Adsorption removal rate of MB using different types of sponges. (e) UV-vis absorption spectra during photocatalytic degradation of MB solution (30 mg L^{-1} MB) by AM/MAA/HNTs/β-FeOOH-0.4. (f) Degradation rate of MB. (g) Diagram of the photo-Fenton-catalyzed degradation mechanism.

β-FeOOH-0.4 sponge showed a decrease in the removal of MB from 95% to 88% with the increase in the concentration of MB. With HNTs/β-FeOOH-0.4, the adsorption of MB by the AM/MAA/HNTs/β-FeOOH-0.4 sponge decreased. This may be due to the fact that the powder has a greater chance of contacting MB molecules in a short period of time than the block sponge at the same stirring speed. MB dye was chosen to analyze the photodegradation ability of AM/MAA/HNTs/β-FeOOH-0.4 sponges. After waiting until the adsorption equilibrium of AM/MAA/HNTs/β-FeOOH-0.4 in a dark environment, the MB solution was almost completely degraded within 30 min after turning on the visible light equipment (Fig. 5f). The UV-vis absorption spectra of the MB solution under different irradiation times are shown in Fig. 5e, from which it can be seen that the MB solution has a strong absorbance at 664 nm, which has almost completely disappeared within 30 min of light exposure. In addition, with the prolongation of the degradation time, the MB solution gradually became trans-

parent, which indicated that the conjugated chromophore structure of the MB dye was destroyed. It was completely degraded to organic or inorganic small molecules or ionic products, and its photocatalytic mechanism is shown in Fig. 5g.[34]

3.4 Emulsion separation

In order to better realize the separation of emulsions, an AM/MAA/HNTs/β-FeOOH-0.4 sponge was cut into thin slices with a thickness of 3 mm. A circular separation membrane was formed by the extrusion of an emulsion separation device (Fig. S2b†). The emulsion was turbid before separation and colorless and transparent after separation. The average particle size of the cyclohexane oil-in-water emulsion was 421 nm (Fig. 6a). The AM/MAA/HNTs/β-FeOOH-0.4 sponge showed good adsorption of methylene blue. As shown in Fig. S3,† the AM/MAA/HNTs/β-FeOOH-0.4 sponge as the separation membrane could effectively separate the methylene blue solution ($C_{MB} < 10$ mg L^{-1}). Therefore, an oil-in-water emulsion
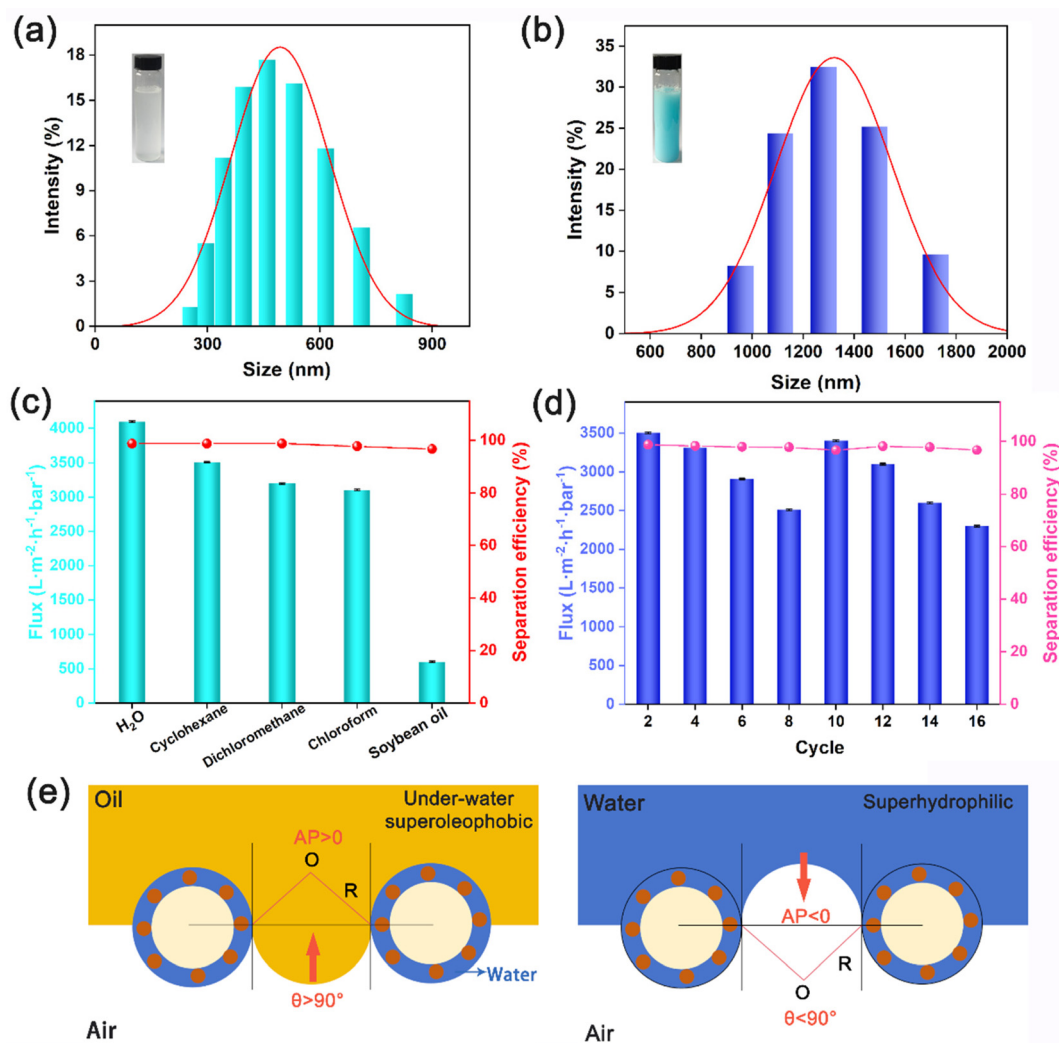

Fig. 6 (a) Oil-in-water emulsion particle size distribution. (b) MB emulsion particle size distribution. (c) Separation efficiency and flux of different types of oil-in-water emulsions. (d) Continuous separation of the cyclohexane oil-in-water emulsion and separation efficiency of Fenton photocatalysis. (e) Diagrams of the emulsion separation mechanism.

(average particle size of 1226 nm) was prepared with an aqueous solution of methylene blue (CMB = 5 mg L^{-1}). The separation process is shown in Fig. S2a.† The membrane was contaminated by methylene blue after separation. Its separation effect was good, and the solution was colorless and transparent after separation. The separation fluxes of cyclohexane emulsion, dichloromethane emulsion, trichloromethane emulsion, and soybean oil emulsion were 3510.6 L m^{-2} h^{-1} bar^{-1}, 3200.9 L m^{-2} h^{-1} bar^{-1}, 3106.5 L m^{-2} h^{-1} bar^{-1} and 601.3 L m^{-2} h^{-1} bar^{-1}, respectively. The separation efficiency for all is greater than 96%, with the highest value reaching 98.9% (Fig. 6c). The flux decreased when increasing the number of emulsion cycle separations, and the flux recovered after the separation membrane was catalyzed by the photo-Fenton reaction (Fig. 6d). The superior wetting selectivity and photo-Fenton catalysis enabled the AM/MAA/HNTs/β-FeOOH-0.4 membrane to achieve significant oil–water separation.[35] The mechanism of emulsion separation is shown in Fig. 6e. The hydrophilic AM/MAA/HNTs/β-FeOOH-0.4 sponge has strong water absorption performance, which makes it possible to form a stable water–solid interface before contact of oil droplets. The stable water–solid interface can effectively prevent oil droplets from adhering to the sponge surface, and the rolling oil droplets eventually form an oil layer.[36] According to Laplace theory,[37] the critical osmotic pressure of oil on the membrane surface is calculated by eqn (3):

$$\Delta p = -2\gamma \frac{\cos \theta}{R} \tag{3}$$

where Δp is the critical osmotic pressure, γ is the oil–water interfacial tension, θ is the contact angle of droplets on the surface of the AM/MAA/HNTs/β-FeOOH-0.4 sponge, and R is the pore size of the modified AM/MAA/HNTs/β-FeOOH-0.4 sponge.

The AM/MAA/HNTs/β-FeOOH-0.4 sponge surface showed good oil repellency after water infiltration, and the θ value of oil droplets was greater than 90°. When $\Delta p > 0$, the AM/MAA/HNTs/β-FeOOH-0.4 sponge wetted by water has a capillary repulsion effect on the dispersed phase of the emulsion. In contrast, due to the super-hydrophilicity of the sponge, the critical permeability of water in the membrane when $\Delta p < 0$ indicates that the composite membrane has a capillary pumping effect on water and can realize rapid pressure-driven molecular water transport.[38]

4. Conclusion

In summary, we treated a polyurethane sponge with β-FeOOH and HNTs to obtain underwater oleophobic AM/MAA/HNTs/β-FeOOH-0.4. The sponge has good chemical resistance and cycling stability. The adsorption and photocatalytic properties of the HNTs/β-FeOOH composite material enable rapid adsorption and degradation of MB (30 mg L^{-1}) within 30 minutes. Underwater oleophobic wettability makes it excellent in separating emulsions. Its maximum flux can reach 3510.6 L m^{-2}

h^{-1} bar^{-1}, and the separation efficiency can reach 98.9%. This work introduces a new method for treating complex wastewater using photocatalytic materials.

Data availability

The authors declare that all data supporting this manuscript are available upon reasonable request.

Conflicts of interest

The authors declare no conflict of interest.

Acknowledgements

References

1 H. Liu, Y. Wang, B. Zhu, H. Li, L. Liang, J. Li, et al., Engineering Dual CO(2)- and Photothermal-Responsive Membranes for Switchable Double Emulsion Separation, Adv. Mater., 2024, 36(19), e2311013.

2 Y. Wang, C. Du, Z. Yan, W. Duan, J. Deng and G. Luo, Rapid demulsification and phase separation in a miniaturized centrifugal demulsification device, Chem. Eng. J., 2022, 446, 137276.

3 B. Wang, X. Luo, Y. Feng, L. Yang, C. Zhang, Z. Dong, et al., Turbo-Synergistic Oily Wastewater Remediation in Bio-Inspired Cone Array Barrel, Adv. Sci., 2022, 9(33), 2204244.

4 D. Yang, Y. Feng, B. Wang, Y. Liu, Y. Zheng, X. Sun, et al., An asymmetric AC electric field of triboelectric nanogenerator for efficient water/oil emulsion separation, Nano Energy, 2021, 90, 106641.

5 H. Gao, S. Chang, J. Liu, Y. Liu, Z. Meng, Y. Song, et al., Ascendant bioinspired emulsion separation materials: From the perspective of droplet movement, Chem. Eng. J., 2023, 474, 145491.

6 Q. Zhang, K. Li, J. Li and Y. Li, Fabrication of hierarchically porous superhydrophobic polystyrene foam for self-cleaning, oil absorbent, highly efficient oil–water separation, Chem. Eng. J., 2024, 483, 149338.

7 A. A. Al-Shamrani, A. James and H. Xiao, Destabilisation of oil–water emulsions and separation by dissolved air flotation, Water Res., 2002, 36(6), 1503–1512.

8 J. Yan, J. Huang, F. Pei, T. Bai, Y. Chen, D. Wang, et al., Biomimetic dendritic–networks–inspired oil-water separation fiber membrane based on TBAC and CNC/PVDF porous nanostructures, Chem. Eng. J., 2024, 492, 152307.

9 L. Xu, T. Xu, W. Liu, T. Zuo, T. Wang, Y. Cai, et al., Heterogeneous wettability membrane for efficient demulsi-

© 2025 The Author(s). Published by the Royal Society of Chemistry

RSC Appl. Polym., 2025, 3, 916–925 | 923

fication and separation of oil-in-water emulsions, *Chem. Eng. J.*, 2024, **489**, 151466.

10 B.-Y. Liu, J. Wu, C.-H. Xue, Y. Zeng, J. Liang, S. Zhang, *et al.*, Bioinspired Superhydrophobic All-In-One Coating for Adaptive Thermoregulation, *Adv. Mater.*, 2024, **36**(31), 2400745.

11 C. Hou, W. Liu, L. Du, Y. Li, J. Zhou, S. Lin, *et al.*, Superhydrophobic membrane from double co-crystallization for high-performance separation of water-in-oil emulsion, *J. Membr. Sci.*, 2023, **679**, 121702.

12 W. Dong, F. Liu, X. Zhou, L. Wang, Z. Zhao, Y. Zhou, *et al.*, Superhydrophilic PVDF nanofibrous membranes with hierarchical structure based on solution blow spinning for oil-water separation, *Sep. Purif. Technol.*, 2022, **301**, 121903.

13 Y. Wang, Y. He, J. Yu, L. Zhang, S. Li and H. Li, Alginate-based nanofibrous membrane with robust photo-Fenton self-cleaning property for efficient crude oil/water emulsion separation, *Sep. Purif. Technol.*, 2022, **287**, 120569.

14 W. J. Lee, Y. Bao, A. Liangdy, X. Hu and T.-T. Lim, Insights into the synergistic role of catalytic ceramic membranes for ozone and peroxymonosulfate activation towards effective recalcitrant micropollutant degradation and mineralization, *Chem. Eng. J.*, 2022, **430**, 132921.

15 H. Yang, B. Zhu, L. Zhu, Z. Zeng, G. Wang and Z. Xiong, Efficient Fenton-Like Catalysis Boosting the Antifouling Performance of the Heterostructured Membranes Fabricated via Vapor-Induced Phase Separation and In Situ Mineralization, *ACS Appl. Mater. Interfaces*, 2021, **13**(36), 43648–43660.

16 Y. Xu, W. Lin, H. Wang, J. Guo, D. Yuan, J. Bao, *et al.*, Dual-functional polyethersulfone composite nanofibrous membranes with synergistic adsorption and photocatalytic degradation for organic dyes, *Compos. Sci. Technol.*, 2020, **199**, 108353.

17 B. Chen, Y. Wang, S. Shen, W. Zhong, H. Lu and Y. Pan, Lattice Defects and Electronic Modulation of Flower-Like Zn3In2S6 Promote Photocatalytic Degradation of Multiple Antibiotics, *Small Methods*, 2024, **8**(10), 2301598.

18 Z. Ji, Y. Wu, L. Liu, W. Zheng, M. Wu, Y. Li, *et al.*, Inkjet-Printed Flexible and Transparent Ti3C2T/TiO2 Composite Films: A Strategy for Photoelectrically Controllable Photocatalytic Degradation, *Small Struct.*, 2024, **5**(11), 2400214.

19 D. Zhang, X. Han, X. Kong, F. Zhang and X. Lei, The Principle of Introducing Halogen Ions Into β-FeOOH: Controlling Electronic Structure and Electrochemical Performance, *Nano-Micro Lett.*, 2020, **12**(1), 107.

20 K. Wan, T. Fang, W. Zhang, G. Ren, X. Tang, Z. Ding, *et al.*, Enhanced antimony removal within lamellar nanoconfined interspaces through a self-cleaning MXene@CNF@FeOOH water purification membrane, *Chem. Eng. J.*, 2023, **465**, 143018.

21 N. Sreedhar, M. Kumar, S. Al Jitan, N. Thomas, G. Palmisano and H. A. Arafat, 3D printed photocatalytic feed spacers functionalized with β-FeOOH nanorods inducing pollutant degradation and membrane cleaning capabilities in water treatment, *Appl. Catal., B*, 2022, **300**, 120318.

22 S. Tian, Y. Zhang, Q. Sha, X. Zhang, T. Yang, X. Yan, *et al.*, PPS/TA-PEI/β-FeOOH membranes with powerful photo-Fenton self-cleaning capability for efficient oil–water emulsion separation, *Chem. Eng. J.*, 2024, **485**, 150069.

23 Y. Feng, X. Chen, R.-R. He, Z. Liu, Y. M. Lvov and M. Liu, The Horizons of Medical Mineralogy: Structure-Bioactivity Relationship and Biomedical Applications of Halloysite Nanoclay, *ACS Nano*, 2024, **18**(31), 20001–20026.

24 L. Zhou, G. Xiao, Y. He, J. Wu, H. Shi, X. Yin, *et al.*, Multifunctional composite membrane with strong photocatalysis to effectively separate emulsified-oil/dyes from complex oily sewage, *Colloids Surf., A*, 2022, **643**, 128733.

25 W. Ahmad, Y. Hou, N. Ahmad, K. Wang, C. Zou, Z. Wan, *et al.*, Sr-induced Fermi Engineering of β-FeOOH for Multifunctional Catalysis, *Small Methods*, 2024, **8**(9), 2301434.

26 Z. Jiang, S. Sun, J. Liu and X. Sun, Recent Advances of Halloysite Nanotubes in Biomedical Applications, *Small*, 2024, **20**(2), 2306169.

27 P. Fan, X. Wu, J. Zeng, L. Li, K. Qian, H. Qin, *et al.*, Resolve the species-specific effects of iron (hydr)oxides on the performance of underlying zerovalent iron for metalloid removal: Identification of their key properties, *J. Hazard. Mater.*, 2024, **477**, 135378.

28 Z. Liu, J. Yang, J. Jing, X. Zhang, Y. Fu, M. Li, *et al.*, Interfacial assembly of a durable superhydrophobic polyurethane sponge with "scalelike" structures for efficient oily emulsion separation, *J. Mater. Chem. A*, 2023, **11**(34), 18081–18088.

29 H. Liu, H. Zhong, Q. Yuan, R. Yang, M. Kim, Y. H. T. Chan, *et al.*, Roll-to-Roll Manufacturing of Breathable Superhydrophobic Membranes, *Small Methods*, 2024, **8**(12), 2400038.

30 Y. Lian, H. Wang, L. Liu, L. Guan, M. Lin, Q. Li, *et al.*, Highly Stretchable, Transparent Hydrogel for Electromagnetic Interference Shielding, *Small Struct.*, 2024, 2400486.

31 Y. Liu, X. Yang, J. Ai, Q. Shang, D. Wang and G. Liao, Amino-functionalized biomass-based aerogel derived from waste reed converted into an efficient photocatalyst after adsorption of Cu2+, *Chem. Eng. J.*, 2023, **474**, 145586.

32 Ç. Güngör and M. Ece, Competitive adsorption of VOCs (benzene, xylene and ethylbenzene) with Fe3O4@SiO2-NH@BENZOPHENONE magnetic nanoadsorbents, *Chem. Eng. J.*, 2023, **475**, 146034.

33 R. Solís-Rodríguez, R. Pérez-Garibay, O. Alonso-González and D. Mendieta-George, Enhancing the arsenic adsorption by controlling the zeta potential of Zn(OH)2 flocs, *J. Environ. Chem. Eng.*, 2021, **9**(5), 106300.

34 S. Su, Y. Liu, X. Liu, W. Jin and Y. Zhao, Transformation pathway and degradation mechanism of methylene blue through β-FeOOH@GO catalyzed photo-Fenton-like system, *Chemosphere*, 2019, **218**, 83–92.

35 S. Huang, R. H. A. Ras and X. Tian, Antifouling membranes for oily wastewater treatment: Interplay between wetting and membrane fouling, *Curr. Opin. Colloid Interface Sci.*, 2018, **36**, 90–109.

36 J. Ge, J. Zhang, F. Wang, Z. Li, J. Yu and B. Ding, Superhydrophilic and underwater superoleophobic nanofibrous membrane with hierarchical structured skin for effective oil-in-water emulsion separation, *J. Mater. Chem. A*, 2017, **5**(2), 497–502.

37 A. Lafuma and D. Quéré, Superhydrophobic states, *Nat. Mater.*, 2003, **2**(7), 457–460.

38 M. Cao, F. Xiao, Z. Yang, Y. Chen and L. Lin, Purification of oil-containing emulsified wastewater via PAN nanofiber membrane loading PVP-UiO-66-NH2, *Sep. Purif. Technol.*, 2022, **297**, 121514.